Experimental Testbed of Post-OFDM Waveforms Toward Future Wireless Networks

Rafik Zayani, Hmaied Shaiek, Xinying Cheng, Xiaotian Fu, Christophe Alexandre, Daniel Roviras

IEEE Access
Multidisciplinary | Rapid Review | Open Access Journal

Date of publication xxxx 00, 0000, date of current version xxxx 00, 0000.

Digital Object Identifier 10.1109/ACCESS.2018.DOI

Experimental Testbed of post-OFDM Waveforms Toward Future Wireless Networks

RAFIK ZAYANI[1,2], (Member, IEEE), HMAIED SHAIEK[2], (Member, IEEE), XINYING CHENG[2], XIAOTIAN FU[2], CHRISTOPHE ALEXANDRE[2], (Member, IEEE) DANIEL ROVIRAS[2], (Senior Member, IEEE)

[1]Carthage University, Sup'Com, Innov'COM, Ariana 2083, Tunisia
[2]CNAM, CEDRIC/LAETITIA, Paris 75003, France

Corresponding author: Rafik Zayani (e-mail: rafik.zayani@supcom.tn).

This work has been performed in the framework of the WONG5 project, receiving funds from the French National Research Agency (ANR) under the contract number ANR-15-CE25-0005-02

ABSTRACT This paper details an experimental testbed conceived for studying the capability of new multicarrier waveforms to accommodate 5G requirements. Testbed experiments are done with an implementation of cyclically prefixed orthogonal frequency division multiplexing (CP-OFDM) and its most promising enhancements, i.e., weighted overlap and add based OFDM (WOLA-OFDM) and block-filtered OFDM (BF-OFDM), with configurable universal software radio peripherals (USRPs) based software defined radio (SDR) prototype. These experiments are done in a realistic laboratory-like environment where capabilities of the selected waveforms to accommodate 5G requirements are evaluated while focusing on the optimization of the energy efficiency. On one hand, we provide details and deign guidance to improve energy efficiency and robustness of the studied waveforms through new approaches of digital predistortion (DPD) and peak-to-average power ratio (PAPR) reduction in presence of RF power amplifier (RF PA). In particular, we focus on the mitigation of in-band and out-of-band non-linear distortions and their effects on power spectrum density (PSD) and bit error rate (BER), respectively. It has been demonstrated that the combination of PAPR reduction and DPD allows the transmitter to significantly improve the spectrum localization without sacrificing the in-band and out-of-band waveform quality, while achieving high power efficiency, thus operating the PA very close to its saturation region, as well. On another hand, we address the impact of the lack of synchronism between transmitters on the performance of the selected waveforms, which is of special relevance for future 5G massive machine type communications (mMTC) applications. Experimental results show that BF-OFDM and WOLA-OFDM would permit the accommodation of 5G requirements when RF PA issues are tackled. In some specific scenarios, ideal spectrum utilization can be realized by these waveforms, using only one tone as guard band while keeping good energy efficiency.

INDEX TERMS 5G, mMTC, Multicarrier Waveforms, CP-OFDM, WOLA-OFDM, BF-OFDM, RF PA, PAPR, DPD, Asynchronous multi-user access, Testbed.

I. INTRODUCTION

Research, development and standardization activities are in full action toward the fifth/next generation (5G) wireless networks [1], which will have to accommodate, in addition to mobile broadband applications, various new service regimes arising with new fields of applications. Indeed, usage scenarios for international mobile telecommunication (IMT) for 2020 and beyond has been categorized into three broad groups of use cases [2]: enhanced mobile broadband (eMBB), massive machine type communications (mMTC) (also known as Internet of Things (IoT)), and ultra-reliable and low latency communications (URLLC). In particular, mMTC and URLLC require critical capability objectives such as 10^6 devices$/km^2$ connection density, ultra high energy efficiency, low cost terminals, 1 ms latency and mobility up to 500 km/h [3], presenting serious challenges on 5G commercial deployments [4].

To meet these design goals, the third generation partner-

ship project (3GPP) has launched the standardization activity for the first phase 5G system in Release 15 named New Radio (5G-NR) in 2016 [5], which has been published in December 2017 and is mainly dedicated to 5G-NR eMBB and Fixed Wireless Access (FWA) [1]. Regarding physical layer specifications, the major innovation of release 15 with respect to former standards is the support of mixed numerology which allows the service to choose between a set of supported subcarrier spacing (SCS) and symbol durations that better fit its needs. Due to these new requirements, the concept of transparent waveform processing, i.e., transmitter (Tx) and receiver (Rx) use different waveform processing techniques, is primordial to address challenges of 5G [6]. 5G-NR system evolution through transparent transparent Tx and Rx processing enhancement has been discussed and analyzed in [7].

To address this wide range of requirements with a unified physical layer in the same system bandwidth, the consensus among researchers in both academia and industry is that enhanced multicarrier waveforms (MWFs) are required to accommodate heterogeneous service requirements in a flexible way [2]. Indeed, in the era of 5G, it is required to seek possible enhancements to the traditional cyclically prefixed orthogonal frequency division multiplexing (CP-OFDM) and its low peak-to-average power ratio (PAPR) variant discrete Fourier transform spread OFDM (DFT-s-OFDM), which have consequently shaped the success of the 4G long-term evolution (LTE). Further enhancements aim to provide better performances over multi-services and multi-user scenarios with potentially a high energy efficiency.

In this regard, notable waveforms have been introduced and investigated to address the major limitations of the classical CP-OFDM in challenging new spectrum use scenarios, like asynchronous multiple access, as well as the support of mixed numerology which allows the service to choose between a set of supported subcarrier spacing (SCS) and symbol duration.

A first class of these MWFs gathers the ones that adopt a per-subcarrier pulse-shaping to reduce out-of-band (OOB) emission and increase bandwidth efficiency and relaxed synchronization requirements: filter-bank multi-carrier (FBMC) [8] has been heavily studied. However, FBMC exhibits high algorithmic and computational complexities and it is poorly compatible to MIMO making it not attractive for next 5G networks [9]. In addition, FBMC provide excellent OOB reduction for each subcarrier, but this is actually not required, since resource allocation and adaptive coding and modulation schemes are commonly applied with a resource block (i.e. a group of subcarriers) as the basic unit [10]. In this work, we have discarded this class of MWFs due to their excessive complexity.

Indeed, regarding OFDM based advanced waveform (WF), two candidate classes, sub-band-filtered CP-OFDM schemes and time-domain windowing based CP-OFDM processing, are receiving great attention in the 5G waveform development.

As a time-domain windowing based OFDM technique, the weighted overlap and add based OFDM (WOLA-OFDM) [11] has been introduced to the 5G-NR as a low-complexity candidate method (it has nearly computational complexity as the classical CP-OFDM). It has been also demonstrated to allow interesting performance to support asynchronous traffic although it provides meduim performance in terms of OOB emission reduction. In addition, WOLA-OFDM allows transparent design where transmitter (Tx) and receiver (Rx) units use independent waveform processing techniques, which will comply with the 3GPP agreement [1]. It is for these raisons that WOLA-OFDM has been selected for our study.

Another class of sub-band filtering-based waveforms has been investigated, where the universal filtered multicarrier (UFMC) [12], filtred-OFDM (f-OFDM) [13] and fast Fourier transform FBMC (FFT-FBMC) [14] are the most studied. These sub-band-filtered schemes (i.e. apply filtering at sub-band level over single or multiple RBs) are receiving great attention in the 5G waveform development thanks to their ability to address the major limitations of the classical CP-OFDM in challenging new spectrum use scenarios. UF OFDM and f-OFDM have shown to provide close performance to WOLA-OFDM but with a much higher complexity [15]. For this set of WFs, the complexity was a discriminant criterion, implying that these WFs were out the race for the tesbed implementation described in our paper.

Recently, block-filtered OFDM (BF-OFDM) [15] has been introduced to the 5G-NR as a promising sub-band filtered multicarrier based waveform that provides reasonable performance while it has significantly very low complexity [16]. BF-OFDM is built on the concept of sub-band filtering on the top of the baseline CP-OFDM waveform. It has been demonstrated to outperform UFMC and f-OFDM providing very interesting PSD performance, thanks to the PolyPhase Network (PPN) filter banks. BF-OFDM transmitter is very similar to the FFT-FBMC one where the filtering operation is applied with a PPN where a number of carriers (=number of RBs) are processed by a filter bank stage. However, BF-OFDM receiver is reduced to simple FFT (i.e. no more than the classical CP-OFDM receiver). It is for this reason that we have considered BF-OFDM for the development of our demonstrator.

Another flexible and effective frequency-domain filtering scheme [10], based on fast-convolution (FC), was proposed for sub-band f-OFDM as a candidate waveform for 5G-NR system development. This is an extension of some earlier works on exploiting the FC filtering approach for advanced multicarrier waveforms in flexible and efficient manner [17] [18]. The proposed FC-F-OFDM has been compared in [19] to WOLA-OFDM, UF-OFDM and f-OFDM in terms of performance and complexity and obtained results have shown that FC-F-OFDM design can achieve the performance requirement and significantly exceeds the overall radio link performance of the other waveforms while maintaining very low complexity. Moreover, FC-F-OFDM has a good processing flexibility allowing to construct arbitrary sub-band

configurations, as groups of RBs [7].

Even FC-F-OFDM was a good candidate for advanced filtered multicarrier waveform, it has not been considered in this study. When came the time for choosing within the large set of filtered multicarrier waveforms available in the literature for test-bed implementation, we decided to implement only three WFs in the context of Critical-Machine Type Communications. The chosen waveforms were: (1) CP-OFDM because it has been chosen for 5G and also as a reference basis, (2) WOLA-OFDM because of similar complexity as CP-OFDM and good performances in asynchronous scenarios and (3) BF-OFDM because of the good frequency localization, good performance in asynchronous scenarios and the fact that the receiver was a classical CP-OFDM one. In terms of complexity and OOB, BF-OFDM and FC-F-OFDM have quite similar performances. The fact that the BF-OFDM receiver could be a classical CP-OFDM receiver guided our final choice.

Despite the mentioned MWFs advantages, they still suffer from high PAPR of the modulated signal. Consequently, they lose rapidly their good frequency localisation properties when non-linear RF power amplifiers (RF PA) are deployed.

Motivated by these considerations, it is encouraged to concentrate on more careful and thoughtful design, evaluations, realizations and comparison of CP-OFDM waveform and its most promising enhancements, i.e., WOLA-OFDM and BF-OFDM especially in experimental testbed. It is worth to mention the following contributions:

- Levanen et al. [7] provide a basic framework of how transmitter and receiver units that can be independently applied and evaluated in the context of transparent design and an extensive set of examples of the achieved radio link performance with unmatched transmitter and receiver waveform processing,
- In [4], authors describe field-test experiments carried out with an implementation of the BF-OFDM and the feasibility of the use of mixed numerology for 5G,
- Guan et al. [20] report a field in time division duplex downlink (TDD-DL) conducted on a configurable testbed in a real-world environment for the performance evaluations of CP-OFDM, Windowing-OFDM and filtered-OFDM,
- Zayani et al. [21] present experimental testbed to evaluate the impact of RF PA on the performance of CP-OFDM, WOLA-OFDM and BF-OFDM.

Compared to the above contributions, this paper presents testbed experiments done with an implementation of CP-OFDM, WOLA-OFDM and BF-OFDM, with configurable universal software radio peripherals (USRPs) based software defined radio (SDR) prototype [22] [23]. These experiments are done in a realistic laboratory-like environment where capabilities of the selected waveforms to accommodate 5G requirements are evaluated while focusing on the optimization of the energy efficiency. These experiments are crucial in order to convince evidences of advanced multicarrier waveform technology feasibility using real-world environment imposing some RF imperfections: RF power amplifier nonlinearities, IQ Imbalance and Mirror-Frequency Interference, Phase noise and Mixer and A/D converter nonlinearities.

Indeed, the link performance results are provided for two scenarios : down-link (DL) and uplink (UL) following the experimentation cases. Scenario 1 corresponds to interference free DL with nonlinear amplification and scenario 2 defines an asynchronous UL case. Therefore, these scenarios are envisaged to address the following main characteristics :

- Higher energy- and spectrum- efficiency (DL case) : 5G energy efficiency is expected to be considerably optimized than its precedent for mMTC and URLLC. In this regard, these latter should use low-cost and low-size PA that should be operated near its saturation region (i.e., nonlinear region). This will imply in-band and out-of-band distortions, damaging then the good spectral confinement of the selected MWFs. Thus, a very large bandwidth should be reserved as guard bands for the signal to meet the spectrum mask and adjacent channel power ratio (ACPR) requirement (i.e., poor efficient spectrum utilization). Towards very good energy- and spectrum- efficiency, PA nonlinearities have to be well addressed and compensated, making possible to reduce guard-bands tremendously while keeping more efficient energy utilization,
- uplink (UL) Asynchronous transmissions: In LTE, with OFDMA we need all the signals coming up, from user equipments (UE), to the base station are lined-up in order to mitigate inter-carrier interference (ICI). To maintain this stringent synchronization a heavy overhead have to be associated which is not favorable for mMTC service. It is important to evaluate the capability of the selected 5G waveforms to support asynchronous transmissions in a realistic environment.

Thus, The main contributions of this paper are :

- Experimental testbed results: We believe that measurement results in a real-world environment are primordial in order to convince evidences of technology feasibility. In this work, we aim firstly to build a practical and flexibly configurable testbed, as a general platform for research, development and validation for several 5G physical layer technologies. We provide details and guidance on the testbed design and implementations which will be references for the readers who are wiling to conduct experimentation testbeds,
- Design guidance to improve energy efficiency and robustness: we present testbed experiments done in a realistic laboratory-like environment using real-world RF power amplifier. On one hand, we characterize digital predistortion (DPD) to linearize the RF PA. On another hand, we study the PAPR reduction of the MWFs time-domain signals using tone reservation (TR) [24] and selective mapping (SLM) [25], which are deeply studied in literature. Since BF-OFDM has a different structure compared to CP-OFDM and WOLA-OFDM, we intro-

duce modified TR and SLM techniques that are more adequate to BF-OFDM than the classical ones. In particular, we focus on the combination of the proposed PAPR reduction and DPD techniques in order to mitigate the in-band and out-of-band nonlinear distortions caused by the real RF PA while improving the energy efficiency,
- Multi-user access scheme: We study, through the developed testbed, the capability of the 5G waveform of handling multi-user signals when there is imperfect synchronization in time domain. We provide further discussions and comparisons of the selected waveforms CP-OFDM, WOLA-OFDM and BF-OFDM, with corresponding parameter selections. More precisely, we consider the coexistence of two users which are asynchronously transmitting in adjacent bands using the same transmit power per subcarrier. We also provide insights on the impact of several important system parameters, e.g. guard bandwidth and filter design.

The rest part of this paper is structured as follows. Section II provides an overview of the tesbed. In particular, the detailed baseband processing of CP-OFDM, WOLA-OFDM, BF-OFDM, DPD identification method and introduced PAPR reduction techniques are presented, respectively. In section III, testbed setup is introduced, parameter selections are defined and waveform performance are validated and compared via experimental measurements. The relevant performance, in terms of PSD, normalized mean square error (NMSE) and BER, are discussed. Finally, the conclusion is given in section IV.

Notations : $\mathbb{E}[.]$ stands for the expectation operator and $(.)^*$ denotes the complex conjugate operation.

II. TESTBED OVERVIEW

A. OVERALL ARCHITECTURE

The SDR testbed is realized with two parts, Transmitter (Tx) and Receiver (Rx), to evaluate the performance of several MWFs. The testbed overall architecture is presented in Fig. 1.

The baseband unit is software-based and implemented using MATLAB and it realizes the digital algorithm, e.g., waveform generation, QAM modulation, channel equalization, demodulation, etc. It is worth mentioning that DPD and PAPR reduction methods are also implemented using MATLAB.

For SDR hardware, two separate Universal Software Radio Peripherals (USRPs) devices, NI-USRP-2942R are used as transmitter and receiver, integrating digital/IF/RF units. The USRP has tunable carrier frequencies in the range of 400 MHz to 4.4 GHz and tunable transmission rates to 200 mega samples per second [26]. For synchronization of USRP modules, an external clock is used generating from Marconi Instruments 2051 Digital and Vector Signal Generator, which is crucial for proper operation of multicarrier waveforms. This external clock provides 10 MHz clock signal that is transmitted to the two USRPs. By tuning Tx and Rx USRP devices, we are sure that carrier frequency offset (CFO) between transmitter and receiver is zero. Controlled frequency offset will be generated by shifting in baseband (MATLAB level) the emitted signal.

In order to assure a real-time SDR implementation, we consider a specific computer configuration using two computers (Fig. 2). The computer 1 has two solid state disk (SSD), where the first SSD is dedicated to data storage and is shared with computer 2 using a gigabit ethernet switch and the second SSD is dedicated to the operating system. MATLAB on computer 1 realizes the digital algorithms and commands the GNU-radio that configures and uploads signal to USRP Tx. Also, a C++ program is implemented in computer 1 to get the received signal from the USRP Rx. This received signal is splitted into small packets that will be stored in the shared SSD and will serve for the following analyses in the baseband unit.

Computer 2 realizes the analysis of received signals. It uses shared received packets and gives some visual performance results such as PSD, constellation, NMSE per subcarrier, average NMSE and BER.

Two graphical interfaces have been developed to make our testbed more flexible. On the transmitter side interface, we can choose different configurations, for example, we can select the waveform (CP-OFDM, WOLA-OFDM or BF-OFDM), the input back-off IBO (0, 3, 6, 9 or 12 dB), the PAPR reduction method (TR or SLM), the DPD and we can enable or disable the interferer user. The receiver interface is dedicated to visualize performance results for these different configurations. Thus, we visualize PSD, constellation, NMSE per subcarrier, average NMSE and BER. We have used an additive white Gaussian noise (AWGN) channel without any frequency selectivity in order to clearly see the impact of the RF PA on the performance of the selected MWFs and their robustness to asynchronous transmissions. The RF PA is a solid-state power amplifier (SSPA) PE15A4017 from Pasternack with a bandwidth of 20 MHz to 3 GHz and 27dB Gain [27].

Using this Testbed, we aim to evaluate the capability of the most promising MWFs candidates for future wireless networks (1) to resist to the distortions caused by the RF PA while keeping a good energy efficiency and (2) to support asynchronous multi-user access.

B. BASEBAND PROCESSING PROCEDURE

1) Transceiver Structure

Fig. 3 illustrates the software based baseband processing procedures on the transmitter and receiver. MCM Tx and MCM Rx stand for multicarrier waveform modulation at the transmitter side and receiver side, respectively. This latter realizes the modulation/demodulation for CP-OFDM, WOLA-OFDM and BF-OFDM for the following experiments that will be explained in section II-B2.

For CP-OFDM and WOLA-OFDM, spectral shaping is applied to all active subcarriers: rectangular shaping for CP-OFDM and rectangular shaping plus windowing for WOLA-OFDM. Concerning BF-OFDM, the spectral shaping is ap-

This article has been accepted for publication in a future issue of this journal, but has not been fully edited. Content may change prior to final publication. Citation information: DOI 10.1109/ACCESS.2018.2879375, IEEE Access

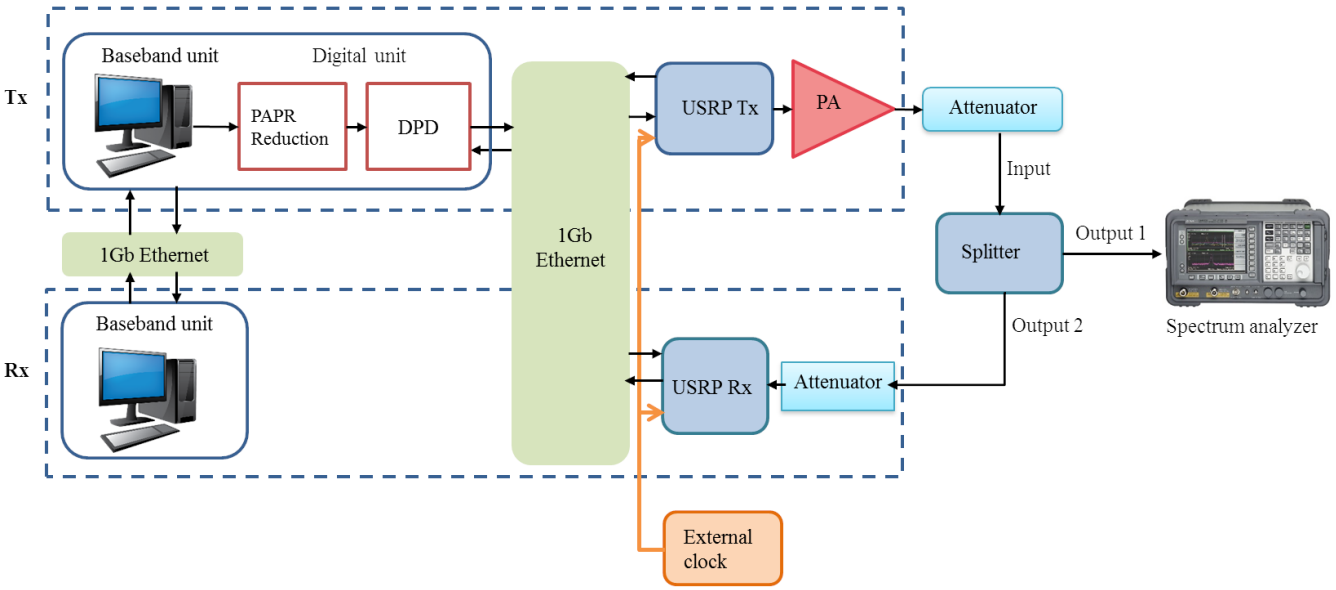

FIGURE 1. Overall architecture.

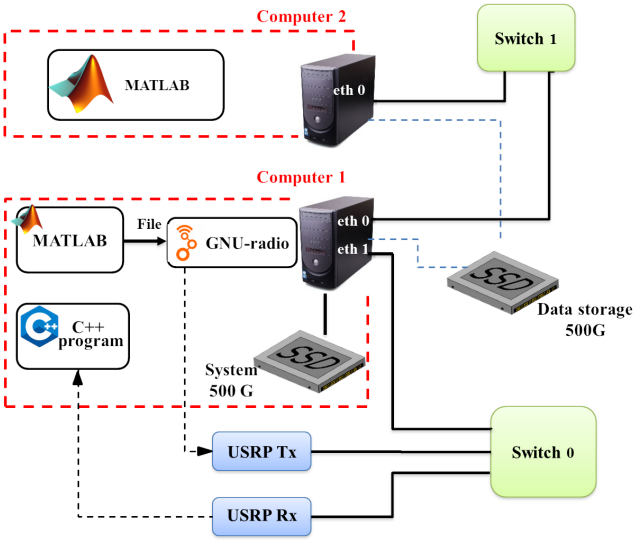

FIGURE 2. Computer architecture.

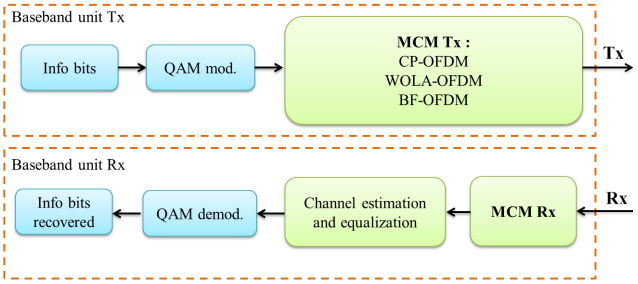

FIGURE 3. Transceiver structure.

plied to groups of $N/2$ subcarriers. In the following, the three MWFs will modulate complex symbols with a maximal size of M_{FFT}. For BF-OFDM, the M_{FFT} complex symbols are divided into M subbands of $N/2$ symbols (i.e. $M_{FFT} = MN/2$).

2) Background of selected MWFs

The classical CP-OFDM is adopted in several wireless standards (e.g. 3GPP-LTE and IEEE 802.11. a/g/n). Its key idea is to split up a stream of complex symbols at high-rate into several lower-rate streams transmitted on a set of orthogonal subcarriers which are implemented using the inverse fast Fourier transform (IFFT). The OFDM transmitted signal can be written as,

$$\underbrace{\mathbf{s_m}}_{[M_{FFT}\times 1]} = \underbrace{\mathbf{F^{-1}}}_{[M_{FFT}\times M_{FFT}]} \underbrace{\mathbf{X_m}}_{[M_{FFT}\times 1]} \quad (1)$$

where, $\mathbf{F^{-1}}$ and $\mathbf{X_m}$ stand for the $M_{FFT} \times M_{FFT}$ IFFT matrix and a $M_{FFT} \times 1$ vector of complex input data symbols, respectively.

Accordingly, the OFDM receiver can be implemented using the fast Fourier transform (FFT). In order to prevent inter symbol interference (ISI), a cyclic prefix (CP) is usually inserted transforming thus the linear channel convolution into circular convolution if the CP is longer than channel impulse response. Therefore, after the FFT operation, the channel equalization becomes trivial through a single coefficient per subcarrier.

In the following, we will discuss notable differences of WOLA-OFDM and BF-OFDM compared to CP-OFDM which consist that, at the transmitter, the CP-OFDM modulated baseband signal is windowed by a well-chosen window function for WOLA-OFDM, or is filtered with a subband-specific filter for BF-OFDM.

This article has been accepted for publication in a future issue of this journal, but has not been fully edited. Content may change prior to final publication. Citation information: DOI 10.1109/ACCESS.2018.2879375, IEEE Access

WOLA-OFDM: Weighted overlap and add based OFDM is chosen because of its capability to support asynchronous transmissions without added complexity [11]. The key idea of WOLA-OFDM is to use windowing to smooth the time-domain symbol transitions, reducing then the OOB emissions. Indeed, it uses a pulse shape with soft edges instead of the conventional usage of rectangular one. The smooth transition of last sample of a given symbol and the first sample of next symbol is performed with point-to-point multiplication of the windowing function and the cyclicly extended symbol. This latter is created by adding cyclic prefix (CP) and cyclic suffix (CS) to its beginning and its end, respectively. To create the CP and CS, we use the last N_{CP} samples and the first W_{TX} samples, respectively, from the given symbol. It is worth to mention that adjacent symbols are overlapped in the edges transition region, i.e. W_{TX} samples, in order to comply with the same overhead as in the classical CP-OFDM.

Although the transmit windowing is used to improve the spectral confinement of the transmitted signal, an advanced windowing is also applied at the receiver side (Fig. 4) in order to suppress the asynchronous inter-user interference that can be captured by the FFT. This process is performed into two steps : (1) For each WOLA-OFDM symbol, we take $M_{FFT} + 2W_{RX}$ samples that are windowed then (2) we apply an overlap and add processing to create the useful M_{FFT} samples.

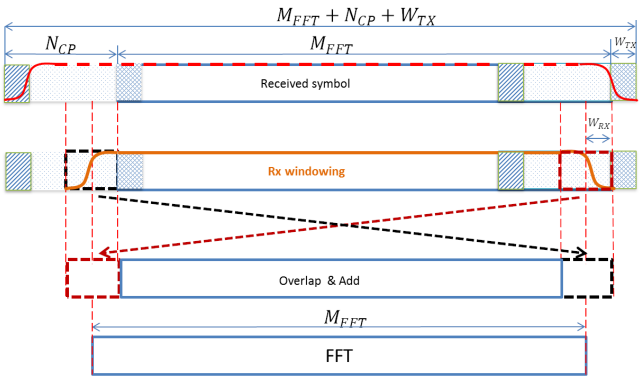

FIGURE 4. WOLA-OFDM processing.

Various windowing functions have been studied and compared [28] for enhancing out-of-band rejection. One straightforward solution is to define edge of the time domain window as a root raised-cosine (RRC) pulse. In this work, we consider the Meyer RRC [29] pulse combining the RRC time domain pulse with the Meyer auxiliary function. It is worth to mention that transmit and receive windowing are independent.

BF-OFDM: Block-Filtered OFDM (BF-OFDM) is a precoded filter-bank multi-carrier modulation that has been introduced in [30], [15]. The precoding stage is performed by means of CP-OFDM modulators and the filtering operation is applied with a polyphase network (PPN). The same precoding scheme was first proposed for FFT-FBMC, introduced in [14], that results in complex receiver scheme. The key idea of BF-OFDM is to slightly increase the transmitter complexity in order to rely on a low-complex CP-OFDM like receiver through the insertion of a filter pre-distortion stage at the transmitter side [4].

BF-OFDM transmitter scheme is shown in Fig. 5. We divide $MN/2$ carriers into M sub-bands and each sub-band contains $N/2$ subcarriers. After framing, we pad the $N/2$ carriers data into N carriers data using zeros. Then we do N-IFFT for each sub-band and append CP in order to keep orthogonality inside sub-bands. After the parallel to serial stage, we separate all symbols into two parts by time index (odd and even). Then, a polyphase network (PPN) process is applied where M carriers processed by a filter bank stage, similarly to usual FBMC transmitters [31]. This filter bank is determined by a prototype filter with an overlapping factor of K. In this investigation, two prototype filters are considere: (1) PHYDYAS [8] and BT-Gaussian [30]. Although the PPN gives good spectral efficiency to BF-OFDM, the filter does distort the transmitted signal. Therefore, a pre-equalization procedure is added before framing in order to reduce this effect caused by filter. Besides, IFFT-based precoding aims as well as overlap and sum stage are used to mitigate intrinsic interference and increase spectral efficiency respectively [32]. All aforementioned process is shown in Fig. 5. Thanks to these techniques, BF-OFDM receiver is able to demodulate the transmitted signal using only a $MN/2$-FFT. It is worth mentioning that every BF-OFDM modulated symbol has a tail that overlaps on its next modulated symbol because of PPN characteristic. For this reason, we do some modified PAPR reduction techniques specially for BF-OFDM which will be explained later.

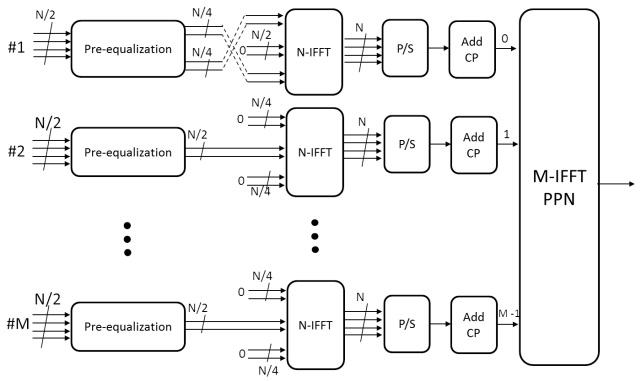

FIGURE 5. BF-OFDM transmitter structure.

The prototype filter plays an important role in the performance of BF-OFDM [33]. It is designed for interference mitigation and orthogonality property improvement. Many filters have been proposed and the most promising ones are Bandwidth-Time (BT)-Gaussian filter and PHYDYAS filter [32]. In this work, we will provide further discussions and comparisons of these prototype filters based BF-OFDM with the other waveforms.

This article has been accepted for publication in a future issue of this journal, but has not been fully edited. Content may change prior to final publication. Citation information: DOI 10.1109/ACCESS.2018.2879375, IEEE Access

3) PAPR Reduction techniques

Peak-to-average power ratio (PAPR) indicates the fluctuation of the transmitted signal amplitude. The PAPR of $\mathbf{s}$ is defined as the ratio of the highest signal peak power to its average power value on a given time-domain interval. In the following, the time-domain interval has been taken equal to a CP-OFDM symbol duration (M_{FFT} samples). Hence, It is given by

$$PAPR(\mathbf{s}) = \frac{\underset{0\leq k\leq M_{FFT}-1}{max}\left[|s_k|^2\right]}{E\left[|s_k|^2\right]}, \qquad (2)$$

A high PAPR means that the transmitted signal will be located, with high probabilities, in the nonlinear and saturation regions of the PA in system. This will affect considerably the system performance while keeping good energy efficiency. In our system, we want to have high power efficiency as well as good performance in terms of spectral localization and robustness to distortion errors. Therefore, reducing PAPR of the transmitted signal is vital for future wireless networks adopting multicarrier waveforms.

Several PAPR reduction techniques have been proposed for OFDM [34]. In this work, we consider tone reservation (TR) [35] and selective mapping (SLM) [36] which are very promising methods.

TR is considered to be an adding signal technique [34] which can be formulated as $PAPR(s+c_{papr}) < PAPR(s)$, where s is the MWF time-domain signal and c_{papr} is the peak-reduction signal generated by reserved tones. TR uses certain number of subcarriers, called peak reserved tones (PRTs), to cancel large peaks of the transmitted signal in time-domain. These PRTs are orthogonal to each other and do not bear any useful data. TR does not need any side information as well as special receiver-oriented operation.

SLM is introduced as a probabilistic technique. The principle of SLM is that the PAPR of an OFDM signal depends on phase shift in frequency domain to an extreme extent. SLM uses the generated candidate vectors with uniformly distributed phase rotation to compute the lowest PAPR for a single symbol. Then mark the vector which gives the lowest PAPR to this symbol and sent $X^v = X \times C^v$, where X is the original frequency-domain symbol, C^v is the marked candidate rotation vector. Each transmitted symbol has its own vector C^v and its index is sent as side information to receiver for demodulation.

These techniques can also be implemented for the other enabling WMFs that we mentioned before because those waveforms can be regarded as advanced version of classical OFDM. However, The classical PAPR reduction schemes, proposed for OFDM, cannot be directly applied to BF-OFDM, as the latter has overlapping signal structure. It is evident form Fig. 6 that BF-OFDM symbols overlap over $KM - M/2$ samples. In this work, we propose a modified TR and SLM for BF-OFDM, by taking into account the overlapping of BF-OFDM signal structure. The key idea is, when reducing the PAPR of the current symbol $s(i)$, we take into consideration the tail of the previous optimized symbol $s(i-1)$, which is the last $KM - M/2$ samples. Results of the new introduced method are discussed in section II-B3 and compared with the classical ones.

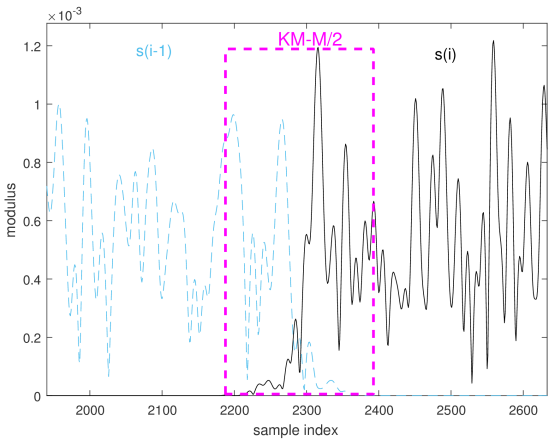

FIGURE 6. BF-OFDM signal structure.

4) Digital Pre-Distortion (DPD)

An important element in the transmit chain of the SDR is the RF power amplifier which amplify the transmitted signal to power levels detectable by the receivers. For high energy efficiency, the PA should be operated close to its saturation region (non-linear region of operation). However, this could drive the device to produce severe amplitude (AM/AM) and phase (AM/PM) distortions. This is the key impairment in multicarrier techniques based communication systems, since these latter suffer from the high PAPR. Introduced nonlinearity leads to spectral re-growth (out of band distortions) outside the allocated bandwidth thus violating the spectral mask. Further, in-band distortions introduced by the nonlinear behaviour of the PA causes increased BER. The AM/AM and AM/PM characteristics indicate the relationship between, respectively, the modulus and the phase variation of the output signal as functions of the modulus of the input one. Then, the amplified signal $u(n)$ can be written as [37]

$$u(n) = F_a(\rho)\exp(jF_p(\rho))\exp(j\phi) \qquad (3)$$

where $F_a(.)$ and $F_p(.)$ stand, respectively, for the AM/AM and AM/PM characteristic and ρ and ϕ are the modulus and phase of the input signal.

To mitigate these nonlinear PA effects, DPD is one of the most promising techniques among all PA linearization ones. It is complementary to PAPR reduction and is adopted to improve the overall linearity of the PA when operated near saturation region. DPD consists on applying to the PA input signal a non-linear function $DPD(.)$ which is the inverse of the PA characteristics. As a consequence, the PA output signal is ideally linearly proportional to the input signal before the predistorter. Various methods have been proposed in literature regarding the extraction of the DPD model,

This article has been accepted for publication in a future issue of this journal, but has not been fully edited. Content may change prior to final publication. Citation information: DOI 10.1109/ACCESS.2018.2879375, IEEE Access

e.g. the PA nonlinearity inverse model or behavioral models with memory, such as: inverse Volterra series [38], the rational function [39], Wiener-Hammerstein systems [40], [41], memory polynomials [42], look-up table (LUT) [43], [44], and neural networks [45]. Another approach of DPD, proposed in [46], aims to identify separately the AM/AM and AM/PM characteristic inverse models. The review of the different methods for DPD is not the main object of this paper and the interested reader is referred to [43] and [44].

In this work, DPD is based on the well-known memoryless polynomial model because of the considered RF PA in our experimental testbed is memoryless. This has been already demonstrated in our previous work [21]. For DPD, we consider the approach presented in [46] that has been shown to give satisfactory performance when used for inverse modeling of nonlinear PA characteristic using inverse learning architecture (ILA) [45].

Using the standard polynomial formulation and imposing the quasi-static constraint results in the lowpass model that referred to as an odd-even model [47]

$$x(n) = \sum_{p=1}^{R} c_p i(n)|i(n)|^{(p-1)} \tag{4}$$

where $i(n)$ is the input signal, R is the number of coefficients and c_p are the complex-valued polynomial coefficients. Usually, c_p are found in the time-domain, either on a sample-by-sample basis using algorithms like least mean squares (LMS) [48] or least squares (LS) [49]. DPD Modeling will be performed using data measured on the considered RF PA through our experimental platform.

III. EXPERIMENTAL RESULTS AND PERFORMANCE EVALUATION

A. EXPERIMENTAL SETUP

Using the testbed presented in the previous section, extensive measurements were performed in a realistic laboratory-like environment. The testbed environment is shown in Fig. 7.

For the measurements, two different scenarios were performed in order to evaluate the performances of the selected waveforms. In scenario 1, the robustness of these WFs against RF PA distortions is evaluated when considering correction techniques like PAPR reduction and DPD for PA linearization. Scenario 2 is dedicated to evaluate the capability of the selected WFs to support asynchronous transmissions. Testbed setups and parameters are provided in Table 1. The user of interest (UoI) occupies 7 resource blocks (RBs), about 1.1 MHz bandwidth from 2.0020 to 2.0031 GHz. Also, we consider a scenario with two co-existing users sharing the available frequency as shown in figure 8. The colored area and the non colored area correspond to time/frequency resources allocated to the user of interest and interfering user. As shown on the figure, on each side of the user of interest, there are 7 RBs, occupying 1.1 MHz bandwidth as interfering user. A guard-band between two users is separating the frequency bands of both users and a timing offset is given to create asynchronism.

TABLE 1. Testbed Parameters

General	
Data frequency band	$2.0020 - 2.0031$ GHz
Sampling rate (F_s)	10 MHz
Subcarriers/RB	$N/2$
Symbol duration	$212\mu s$
Frame size	1000 symbols/frame
Data Constellation	16-QAM
CP-OFDM / WOLA-OFDM	
M_{FFT}	2048
CP length	72
Windowing	Meyer Root Raised cosine
Window length (W_{TX},W_{RX})	$(20, 32)$
BF-OFDM	
M	64
N	64
N_{CP}	4
K	4
Prototype filter	PHYDYAS, Gaussian - BT=1/3

We recall that two scenarios are studied using the testbed. In scenario 1, we active only the user of interest in order to evaluate the spectrum efficiency for different waveforms, the impact of RF PA and the effect of correction techniques. In scenario 2, interferer user is activated and we choose the configuration setup making sure that the RF PA is operated in linear region. This will clearly shows the robustness of the selected waveforms under asynchronous situations.

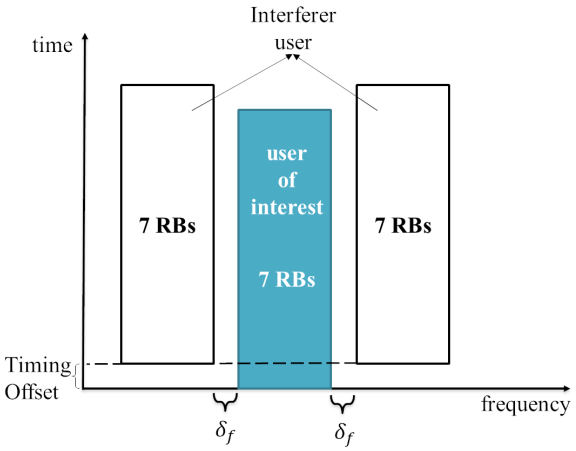

FIGURE 8. Asynchronous scenario.

B. DPD MODELING

In order to identify the digital predistorter model, a digital representation of the PA output envelope is made available to the baseband processing unit using the observation path. The PA output is attenuated, down-converted to IF and converted to baseband using USRP Rx module (see Fig. 9). Then, the data is filtered using a bandpass filter to reject the unwanted

This article has been accepted for publication in a future issue of this journal, but has not been fully edited. Content may change prior to final publication. Citation information: DOI 10.1109/ACCESS.2018.2879375, IEEE Access

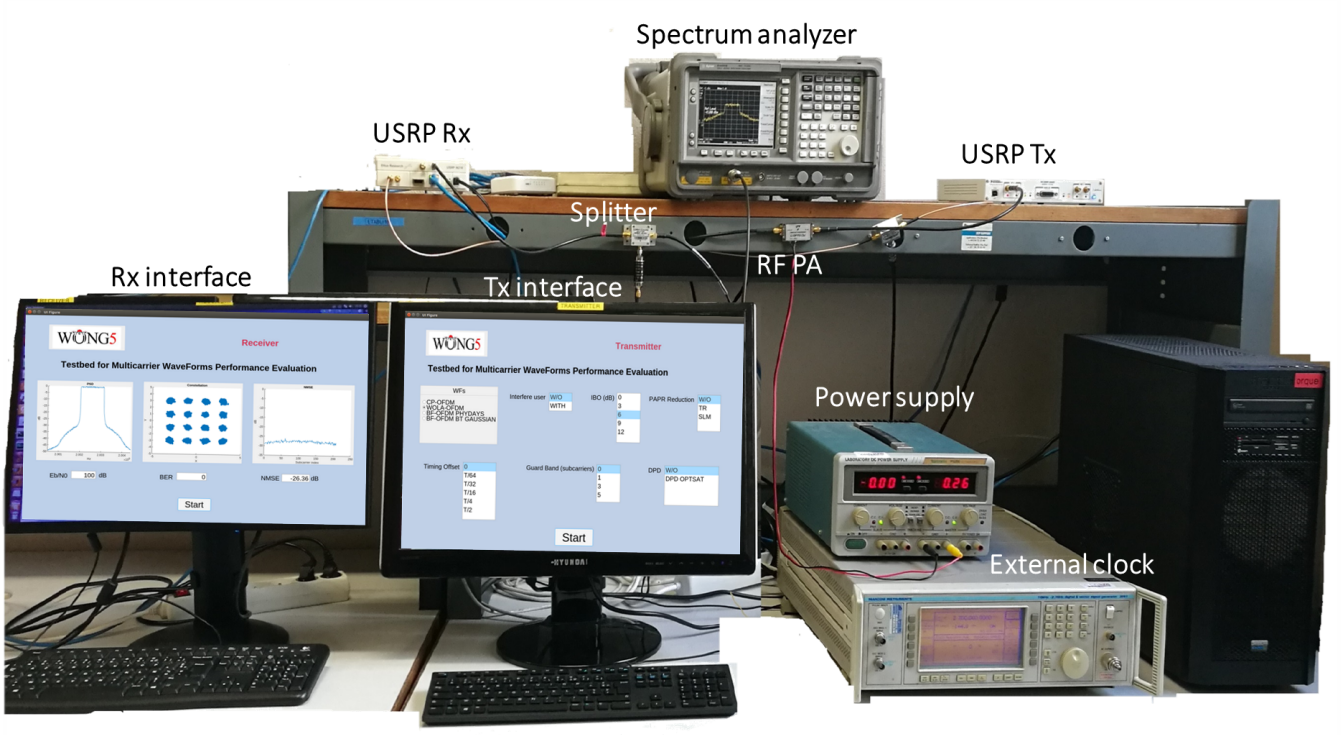

FIGURE 7. Testbed for experimental implementation.

hardware (HW) imperfections like DC component and IQ imbalance. The bandwidth of this filter should at least be three times the transmit data bandwidth that will allow us to observe spectral components generated by nonlinearities up to degree three.

The indirect learning architecture (ILA), which is depicted in Fig. 9, is a simple and efficient architecture to identify the DPD model. A post-inverse of the PA is identified and used as a DPD. The polynomial model in equation (4) was considered using 2048×10^3 samples for both transmit and receive baseband signals and it was evaluated for $R = 30$.

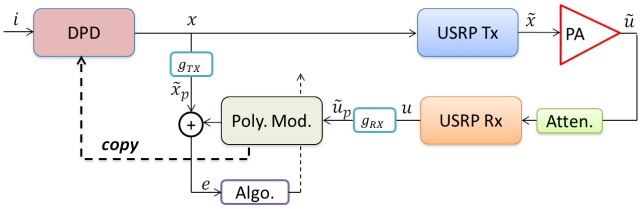

FIGURE 9. Schematic of testbed modules relevant to DPD identification using indirect learning architecture (ILA)

An important condition for proper estimation is that the sequences $x(n)$ and $u(n)$ are time-aligned (Fig. 9). Various elements (analog and digital) in the experimental testbed introduce arbitrary loop delay for the observed signal. Correlation based techniques can be used to estimate and compensate this delay. It is worth mentioning that due to the external synchronisation used for the USRP Tx and USRP Rx modules, the CFO does not exist. Real power amplifier and the estimation algorithm are assumed to operate on scaled version of the PA input $\tilde{x}(n)$ and the PA output $\tilde{u}(n)$. divided by G, the nominal gain of PA. Indeed, the observation path introduces scaling to the observed PA input and output. These effects can be modelled as scaling by real constants g_{TX} and g_{RX}, respectively. g_{TX} and g_{RX} are estimated as follows

$$g_{TX} = \sqrt{\frac{\frac{10^{PindBm/10}}{10}}{\mathbb{E}\left[|x(n)|^2\right]}} \tag{5}$$

where $PindBm$ and $PoutdBm$ denote, respectively, the average power at the input and output of the real PA, which are measured using a spectrum analyzer.

These estimates are used to compute, respectively, $\tilde{x_p}(n) = g_{TX}x(n)$ and $\tilde{u_p}(n) = g_{RX}u(n)$, which then are used by the estimation algorithm as well as the polynomial PA model. In our implementation, more than 2×10^6 samples are used in the DPD coefficient estimation, which is sufficiently large to provide a meaningful LS solution for the model in equation 4. The AM/AM and AM/PM conversion curves of the identified DPD are shown in Fig. 10. We recall that these curves are found from measurements performed using the Pasternack PE15A4017 wideband medium PA [27]. The 1dB compression point (P1dB) is also marked on this plot by circles. It is worth mentioning that, for the AM/AM conversion, the input modulus at which we reach the PA saturation level is 0.45 Volt. Beyond this level, the identified DPD can not perform the inverse of the AM/AM PA characteristic.

This article has been accepted for publication in a future issue of this journal, but has not been fully edited. Content may change prior to final publication. Citation information: DOI 10.1109/ACCESS.2018.2879375, IEEE Access

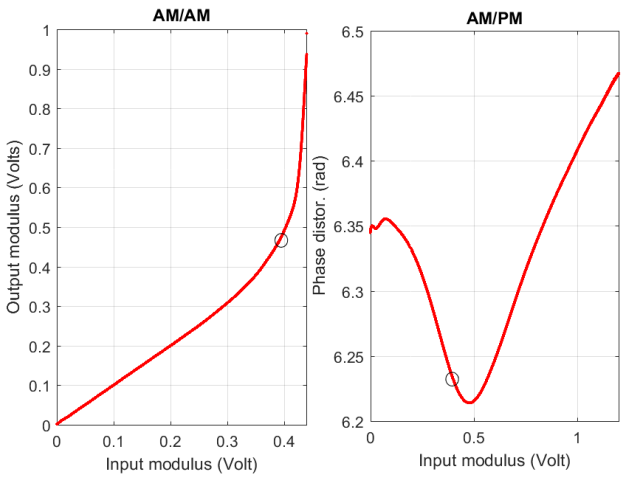

FIGURE 10. AM/AM and AM/PM DPD conversions for PA under test. The black circle marked on the plots correspond to the PA 1dB compression point (P1dB)

In order to validate our approach, the performance of the identified DPD model is studied for the three considered WFs in terms of PSD and BER using our experimental testbed in conjunction with the real RF PA and they are compared to the ones obtained through MATLAB simulation using the characterized PA model performed in [21].

C. SCENARIO 1 : PA NONLINEARITIES

In this subsection, selected sets of measurement results in scenario 1 are reported and analyzed. In particular, we focus on the out-of-bands and in-band effects caused by the RF PA. Performance comparisons of different waveforms, i.e., CP-OFDM, WOLA-OFDM and BF-OFDM are conducted in various cases with different values of IBO, with/without PAPR reduction (SLM or TR) and DPD, respectively.

1) PAPR performance using SLM and TR

Here, we aim to analyze the performance of the introduced modified SLM and TR schemes for BF-OFDM in comparison with CP-OFDM and WOLA-OFDM when classical SLM and TR schemes are used. In MATLAB simulations presented on Figs 11, 12, 13 and 14, complementary cumulative distribution function (CCDF) has been considered as the performance measurement of, respectively, classical SLM, modified SLM, classical TR and modified TR based PAPR reduction. The curves with $'$org$'$ represent the performance of the different WFs without PAPR reduction. Where as, the $'$with SLM$'$/$'$with TR$'$ and $'$with modified SLM$'$/$'$with modified TR$'$ represent the classical SLM/TR and modified SLM/TR, respectively.

In both cases SLM and TR, if we look at the performance of classical methods which follows symbol-by-symbol approach without taking into account the tail of previous symbol, it is obvious that classical SLM/TR is not able to be optimal and could not join the performance of CP-OFDM and WOLA-OFDM with classical schemes. It is noticing from results in Figs. 11 and 13, that the BF-OFDM with classical schemes performs worse than CP-OFDM and WOLA-OFDM and this gap increases with size of V and R with SLM and TR, respectively. Note that V indicates the number of phase rotation vectors and R indicates the number of reserved tones (PRT). The reason that sub-optimality is related to the fact that when we optimize the current symbol without taking into account the overlap structure, whatever improvement that has been achieved for that symbol can probably be affected by its previous symbol. Furthermore, we can clearly see that modified SLM and TR methods, which take into account the tail of previous symbol, provide improvement in PAPR performances and reduce the gap between BF-OFDM and CP-OFDM/WOLA-OFDM (see Figs. 12 and 14) . It is worth mentioning that symbols in WOLA-OFDM are also overlapping but the overlap region is negligible and does not affect the PAPR performance. Thus, we consider only classical schemes of SLM and TR for WOLA-OFDM, which perform as like as with CP-OFDM.

In the following, when PAPR reduction is applied, we have considered $V = 8$ and $R = 16$ (i.e., represents about 7% of activated subcarriers) for SLM and TR, respectively.

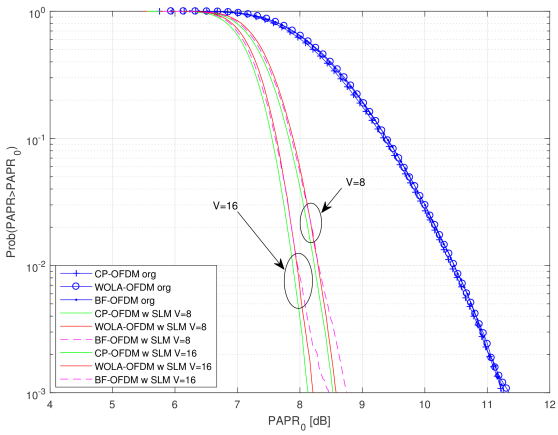

FIGURE 11. PAPR performance of different WFs using SLM method when V=8 and 16.

2) Power Spectral Density (PSD)

Figs 15, 16 and 17 show measured (observed on Agilent ESA E4405B) spectra of the PA outputs for the three MWFs: CP-OFDM, WOLA-OFDM and BF-OFDM when SLM with DPD are considered. The idea here is to analyze the OOB radiation level of each MWF. Results are shown for two values of IBOs 3 and 6 dB. In order to validate our approach, these measured results have been compared to the ones obtained through MATLAB simulations. $'w/ocorrmes'$ denotes measured PSD without any correction. $'wSLM + DPDsim'$ and $'wSLM + DPDmes'$ are, respectively, used to indicate simulated and measured results using SLM with DPD. It is worth to mention that the identified PA model performed in [21] has been used for simulations. Good agreement between

This article has been accepted for publication in a future issue of this journal, but has not been fully edited. Content may change prior to final publication. Citation information: DOI 10.1109/ACCESS.2018.2879375, IEEE Access

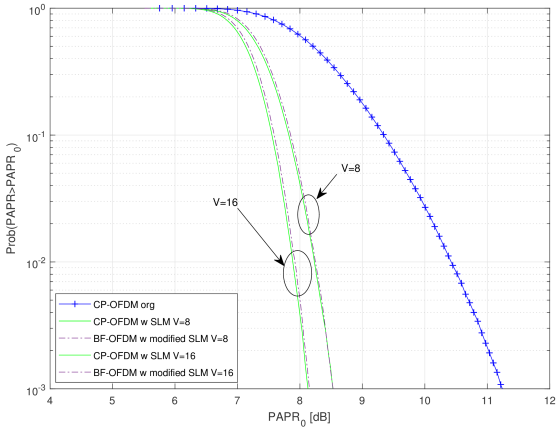

FIGURE 12. PAPR performance of BF-OFDM using modified SLM method when V=8 and 16.

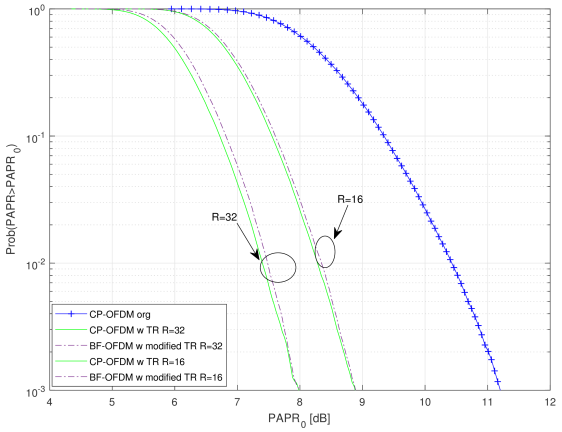

FIGURE 14. PAPR performance of BF-OFDM using modified TR method when R=16 and 32.

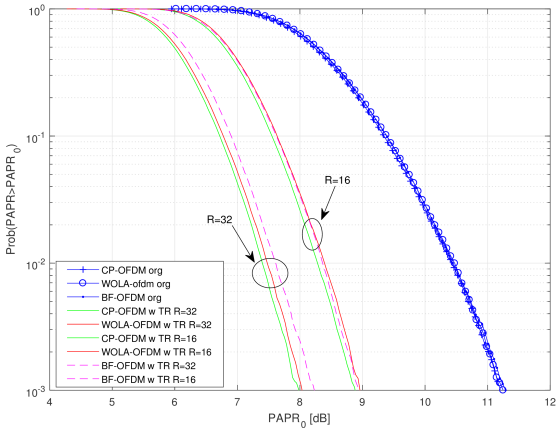

FIGURE 13. PAPR performance of different WFs using TR method when R=16 and 32.

measured and simulated performances proves that this model is efficient and reflects exactly the actual functioning of the real RF PA. We consider an observation bandwidth of three times the main data bandwidth. Two prototype filters, i.e., BT-Gaussian and PHYDYAS, are considered for BF-OFDM that are indicated by $'BF-OFDMBT'$ and $'BF-OFDMPHY'$, respectively. According to these results, we can clearly see a good agreement between simulated spectra and measured ones in the case of all the considered MWfs. This can confirm that our PA/DPD identification method was efficient and validate our experimental results. It is evident that all MWFs have been strongly affected by the RF PA when the energy efficiency is high (IBO=3 and 6dB) and no correction is performed. In this case, advanced MWFs, i.e., WOLA-OFDM and BF-OFDM perform almost as the classical CP-OFDM and they lose their good spectral localization properties. It is worth pointing out that these PA OOB distortions bring a significant amount of interference to adjacent users. Such a behavior significantly reduces the MWFs ability to transmit over multi-user access based networks. In order to overcome this limitation while keeping good energy efficiency, corrections are needed for all MWFs. The same behavioral is shown when the PAPR reduction is performed using TR instead of SLM, the reason why we show only results with SLM.

An improvement is noted when PAPR reduction and DPD are performed for all waveforms. Further, the gain is more pronounced when WOLA-OFDM or BF-OFDM are used. Their performance remains unsatisfactory for low value of IBO, i.e., 3dB, but they can regain their good spectral containment when an IBO of 6dB is considered. Figs 18 and 19 show measured PSD performance comparison of all MWFs when SLM and TR are, respectively, performed with DPD. Here, we can clearly see the significant gain performed with WOLA-OFDM and BF-OFDM compared to CP-OFDM especially for IBO of 6dB. We can also note that BF-OFDM outperforms WOLA-OFDM due to the better spectrum containment provided by the subband filtering used by BF-OFDM. Further, BT-Gaussian based BF-OFDM provides slightly better performance than PHYDYAS based BF-OFDM. For an IBO of 6dB, the CP-OFDM reaches the PSD in the linear case. Nevertheless, because of the rectangular shaping, the PSD localization is poor compared to WOLA-OFDM and BF-OFDM.

3) Adjacent Channel Power Ratio (ACPR)

In order to quantitatively compare spectral regrowth of different MWFs, Table 2 illustrates measured ACPR[1] performance under different configurations ($'w/o'$: without correction, $'SLM/TR + DPD'$: with correction when SLM/TR is performed with DPD) with real RF PA operated at IBOs of 3, 6, and 9dB. As can be observed at IBO=3dB, the scheme with SLM and DPD provides an ACPR gain of 0.5dB for CP-OFDM and about 1dB for WOLA-OFDM and BF-OFDM

[1] ACPR is defined as the ratio of power in the adjacent channels of main channel to the rms power of the transmitted signal in the main channel.

This article has been accepted for publication in a future issue of this journal, but has not been fully edited. Content may change prior to final publication. Citation information: DOI 10.1109/ACCESS.2018.2879375, IEEE Access

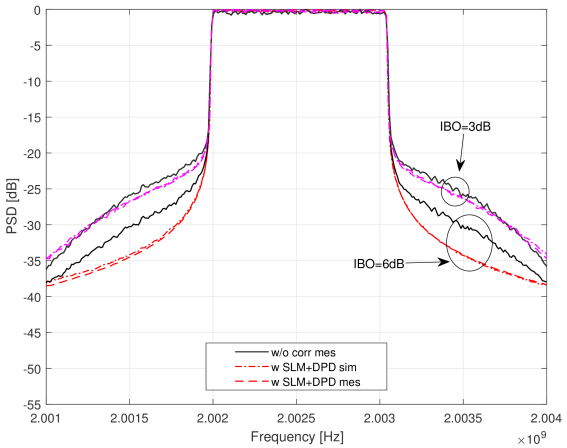

FIGURE 15. PSD performance of CP-OFDM using SLM (V=8) and DPD.

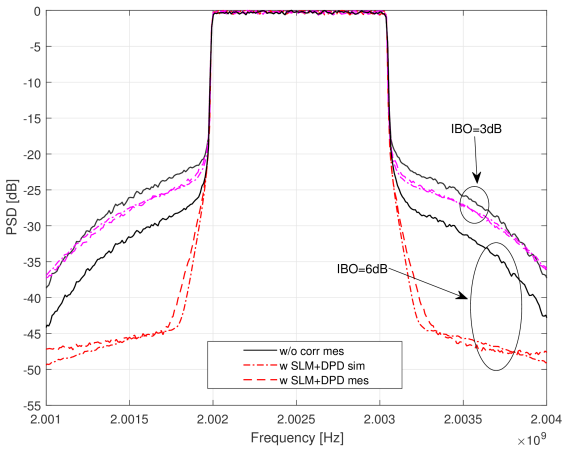

FIGURE 16. PSD performance of WOLA-OFDM using SLM (V=8) and DPD.

compared to the scheme without correction. The ACPR gain increases while increasing the IBO. For example, at IBO of 6 dB, it becomes 3, 7, 9 and 11dB for CP-OFDM, WOLA-OFDM, BF-OFDM PHY and BF-OFDM BT, respectively. As expected, the gain performed with WOLA-OFDM and BF-OFDM is larger than the one provided by CP-OFDM. Further, a 1dB gain is noted when we consider BF-OFDM with BT-Gaussian filter compared to the PHYDYAS one. It is worth mentioning that, for an IBO of 9dB, no significant gain is noted between the two schemes of BF-OFDM, because in this case we reach the noise floor level of the measurement equipment based demonstrator and differences is bellow this level.

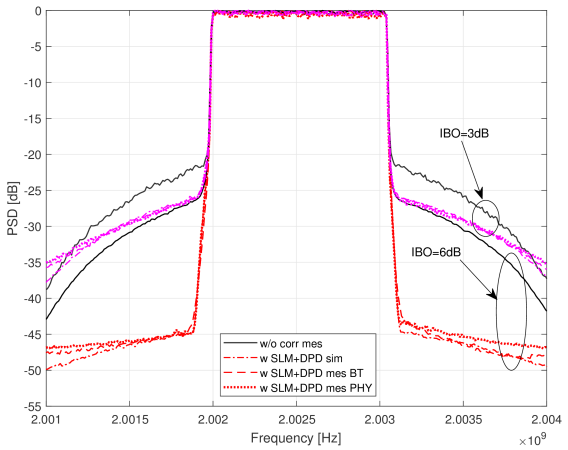

FIGURE 17. PSD performance of BF-OFDM using SLM (V=8) and DPD.

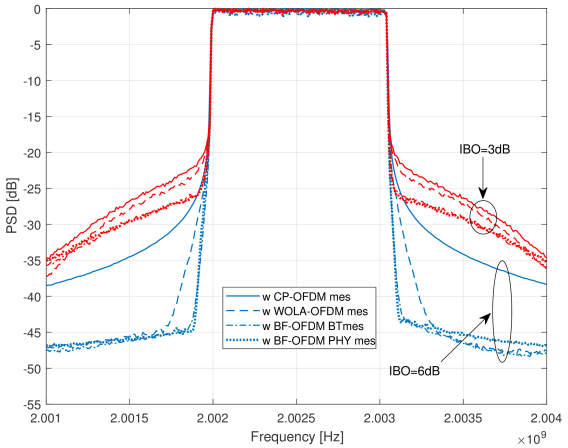

FIGURE 18. PSD performance of different WFs using SLM (V=8) and DPD.

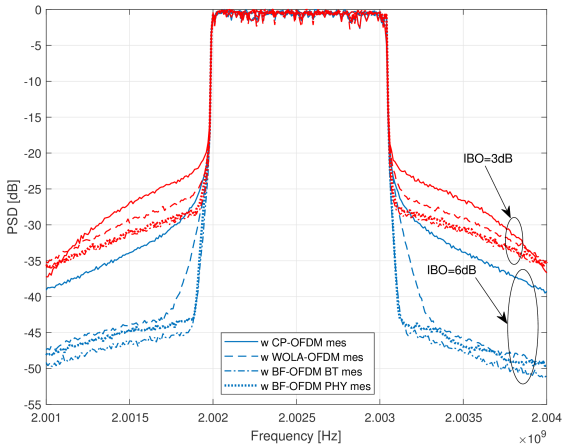

FIGURE 19. PSD performance of different WFs using TR (R=16) and DPD.

This article has been accepted for publication in a future issue of this journal, but has not been fully edited. Content may change prior to final publication. Citation information: DOI 10.1109/ACCESS.2018.2879375, IEEE Access

4) Normalized Mean Square Error (NMSE)

To focus on the impact of in-band RF PA effects on the considered MWFs performance, we measure the NMSE[2] on the decoded symbols. Note that normalized MSE is adopted since it is independent of the constellation scheme. The average NMSE assessed over all data subcarriers is given in Table 3 for all MWFs under different configurations. Again, we note that PAPR reduction and DPD methods provide very interesting enhancements making their crucial in the design of energy efficient MWFs based 5G transmitters. Indeed, at IBO of 3dB, they provide a gain of 2dB and 4dB compared to the case without correction when PAPR reduction is performed by SLM and TR, respectively. Moreover, a gain of 4dB is noted for both PAPR reduction methods at IBO of 6dB where we reach a NMSE of approximately -31dB. The NMSE of -31dB corresponds to the noise floor of the demonstrator in the linear case. In addition, a negligible gain is noted, at IBO of 9dB, compared to the case without correction because we are very close to the noise floor and differences should be below this level. It is worth mentioning that all MWFs have almost the same performance in all cases which explain that each subcarrier in the useful band has been affected by PA nonlinearities regardless the waveform frequency localization.

5) Bit Error Rate (BER)

In order to study the in-band error with different E_b/N_0 regimes, Figs 21 plots measured BER when RF PA is operated at an IBO of 3 and 6dB with and without correction. We can clearly see the improvement provided by the PAPR reduction and DPD schemes compared to the case without correction. Only the the results for CP-OFDM are shown to make the presentation clear but same behaviors have been shown in cases of WOLA-OFDM and BF-OFDM. Fig. 21 compares measured BER of different MWFs when RF PA is operated at an IBO of 3 and 6dB. Again, we can note that WOLA-OFDM and BF-OFDM provide almost the same performance compared to the classical CP-OFDM when PAPR reduction is performed by SLM. The same behavioral has been noted when TR is used. Further, we note a gap in the BER performance, at an IBO of 3dB, compared to the AWGN performance in linear case (indicated by $'theo - AWGN'$). At an IBO of 6dB, BER performance provided by all waveforms is very close to the one performed in linear case. It is worth pointing out that BER floor related to the demonstrator noise floor is not observable for BER $> 10^{-}5$, which represents a significant BER range for wireless communications standards.

D. SCENARIO 2 : MULTI-USER ASYNCHRONOUS ACCESS

Using this scenario, as mentioned previously, we evaluate the robustness of the considered MWFs in multi-user asynchronous access. In order to well assess the performance of these waveforms, we measure the NMSE on the decoded symbols of the user of interest. Both per-subcarrier NMSE (Fig. 22) and the average NMSE (Table 4) obtained over all subcarriers are assessed versus timing offset and guard band. For the average NMSE, we have considered three cases of guard-bands δ_f=0KHz, δ_f=4.883KHz and δ_f=14.65KHz corresponding to 0, 1 and 3 subcarriers spacing. For each guard band, four timing offsets are examinated Δt=0μs, Δt=3.3125μs, Δt=13.25μs and Δt=106μs corresponding to 0, $1/64$, $1/16$ and $1/2$ symbol duration. While for NMSE per-subcarrier curves in Fig. 22, results are given for guard band δ_f of 4.883KHz and timing offset Δt of 106μs. Note that there is no carrier frequency offset (CFO) since USRP modules are perfectly synchronized using the external synchronization.

From results illustrated by Table 4, we clearly show that

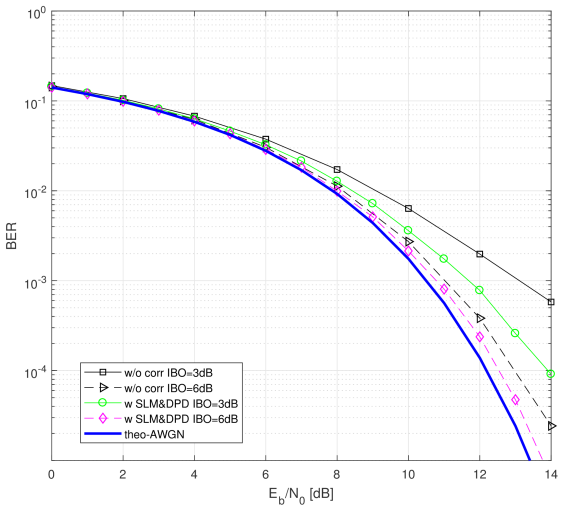

FIGURE 20. BER performance of CP-OFDM using SLM and DPD, 16-QAM.

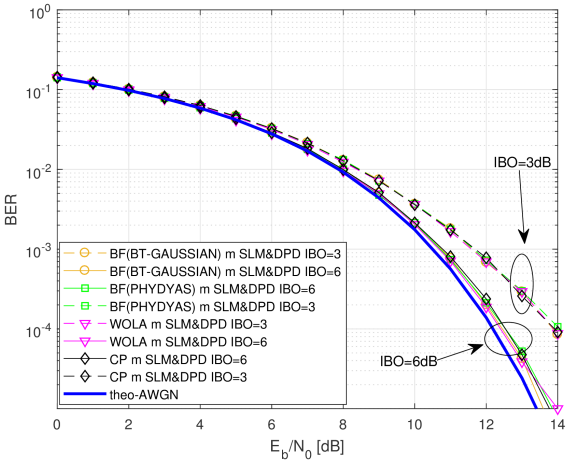

FIGURE 21. BER performance of different WFs using SLM and DPD, 16-QAM.

[2]The NMSE is computed by dividing the MSE by the signal constellation average power.

This article has been accepted for publication in a future issue of this journal, but has not been fully edited. Content may change prior to final publication. Citation information: DOI 10.1109/ACCESS.2018.2879375, IEEE Access

TABLE 2. scenario 1:ACPR [dB] performance of different MWFs under different configurations.

IBO [dB]	3			6			9		
configuration	w/o	SLM+DPD	TR+DPD	w/o	SLM+DPD	TR+DPD	w/o	SLM+DPD	TR+DPD
CP-OFDM	-26.90	-27.30	-27.63	-31.20	-33.36	-33.46	-32.70	-33.47	-33.93
WOLA-OFDM	-27.43	-28.35	-29.22	-34,27	-41.25	-42.94	-40.06	-46.91	-47.48
BF-OFDM PHY	-28.01	-29.82	-30.68	-34.91	-43.89	-45.32	-41.60	-49.18	-49.26
BF-OFDM BT	-28.12	-29.88	-30.97	-35.01	-45.09	-46.43	-41.01	-49.35	-49.41

TABLE 3. scenario 1:NMSE [dB] performance of different MWFs under different configurations.

IBO [dB]	3			6			9		
configuration	w/o	SLM+DPD	TR+DPD	w/o	SLM+DPD	TR+DPD	w/o	SLM+DPD	TR+DPD
CP-OFDM	-20.9	-23.3	-25.1	-26.7	-30.5	-30.6	-30	-31.3	-31.3
WOLA-OFDM	-20.85	-23.16	-25.2	-26.5	-30.4	-30.5	-30.2	-31.2	-31.3
BF-OFDM PHY	-20.9	-23.15	-25.29	-26.7	-30.3	-30.5	-30.4	-31	-31.5
BF-OFDM BT	-20.9	-23.1	-25.5	-26.7	-31	-31	-30.65	-31.3	-31.5

TABLE 4. scenario 2: Average NMSE [dB] performance of different WFs under different configurations.

δ_f (KHz)	0				4.883				14.65			
$\Delta t(\mu s)$	0	3.3125	13.25	106	0	3.3125	13.25	106	0	3.3125	13.25	106
CP-OFDM	-31.5	-31.5	-23.4	-21.6	-31	-31	-23.5	-23	-31.5	-31	-23.8	-24
WOLA-OFDM	-31.5	-30.5	-26.8	-24.8	-31	-30.5	-26.9	-27,2	-31	-30.6	-27.9	-28.5
BF-OFDM PHY	-30	-26.9	-24.8	-23.1	-30	-26.9	-25.2	-25.3	-30	-27	-26	-25.9
BF-OFDM BT	-30.5	-30.5	-25	-22.8	-31	-31	-25.1	-25.5	-30.5	-30.5	-26.1	-26.1

the inter-user interference level depends on the chosen multi-carrier waveform. CP-OFDM exhibits the worst performance when the timing offset does not belong to the CP interval (CP$\approx$ $1/28$ symbol duration). This fact is due to its bad frequency response localization which leads to a severe degradation for CP-OFDM with average NMSE reaching up -21dB, -23dB and -24dB when δ_f = 0KHz, 4.883KHz and 14.65KHz, respectively, in a fully asynchronous scenario (Δt=$106\mu s$). In addition to this negligible enhancement when increasing the guard band, we can see in Fig. 22 that the interference level decreases slowly as the spectral distance between the victim subcarrier and the interferer ones increases.

Regarding WOLA-OFDM case, we can observe better performance compared to CP-OFDM. At Δt=$106\mu s$, one can note a gain of 3dB, 4dB and 4.5dB when δ_f = 0KHz, 4.883KHz and 14.65KHz, respectively. According to results in Fig. 22, the interference level achieved by WOLA-OFDM in the middle of the bandwidth is lower (approximately -34dB) compared to CP-OFDM scheme. These good results are related to the WOLA processing applied at the receiver that is able to suppress inter-user interference resulting from the mismatched FFT capture window.

We move now to BF-OFDM, where additional remarks can be made. Thanks to per-RB filtering, the BF-OFDM shows better performance compared to CP-OFDM. However, the gain of BF-OFDM for the inner subcarriers, located at the middle of the bandwidth, is marginal compared to CP-OFDM. This is a direct consequence of the BF-OFDM receiver which is no more than the classical CP-OFDM receiver (i.e., a simple FFT). Further, at Δt=$106\mu s$, WOLA-OFDM performs better than BF-OFDM and we note a gain of 2dB and 2.5dB when δ_f = 4.883KHz and 14.65KHz, respectively.

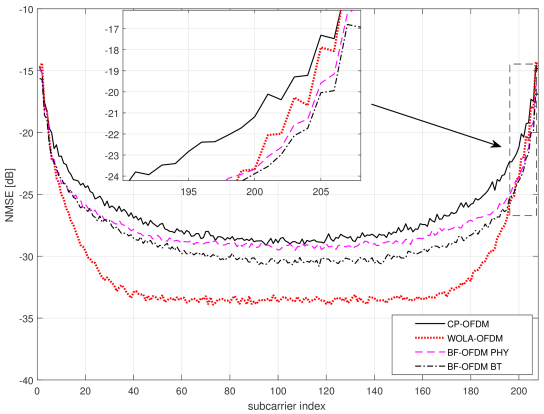

FIGURE 22. scenario 2: NMSE performance of different WFs when $\Delta t = 106\mu s$ and δ_f = 4.883KHz.

However, per-subcarrier NMSE can provide meaningful information about the distribution of asynchronous interference across useful subcarriers, where other conclusions can be made. According to Fig. 22, BF-OFDM provides better protection to the edge subcarriers (in the vicinity of interferer subcarriers) compared to both CP-OFDM and WOLA-OFDM. In such region, the NMSE varies from -16dB when

δ_f = 4.883KHz to -24dB when δ_f = 39.06KHz for BF-OFDM scheme while it varies from -14.2dB to -23dB for WOLA-OFDM scheme when the same band is considered. Thus, BF-OFDM could be more interesting than WOLA-OFDM when few number of RBs will be considered for the user of interest. When comparing the two prototype filters considered for BF-OFDM, one can note that a small gain is performed by BT-Gaussian filter compared to the PHYDYAS one. This is directly related to the filter prototype behavioral.

IV. CONCLUSION

Research, development and standardization activities for the 5G are in full action. As a fundamental component, the underlying post-OFDM waveform is expected to be able to support mixed numerology which allows scalable SCS and symbol duration. In this paper, we present results in a real-world environment in order to convince evidences of advanced multicarrier waveform technology feasibility. Thus, we have built a practical and flexible configurable testbed dedicated to development and validation for several 5G physical layer technologies.

We have provided details and guidance on the testbed design and implementations to improve energy efficiency and robustness of the most promising multicarrier waveforms, i.e. WOLA-OFDM and BF-OFDM. In particular, we have focused on the combination of PAPR reduction and DPD techniques in order to mitigate the in-band and out-of-band nonlinear distortions caused by the real RF PA while improving the energy efficiency. In order to comply with BF-OFDM structure, we have introduced new PAPR reduction techniques that take into account the overlapping structure of BF-OFDM signal. Testbed results demonstrated that the combined DPD and PAPR reduction allows the transmitter to significantly improve the spectrum localization without sacrificing the in-band and out-of-band waveform quality, while operating very close to the PA saturation level, thus achieving high power efficiency as well. The results are generally applicable to all spectrally localized MWFs.

Furthermore, the developed testbed has been dedicated to evaluate the capability of the selected waveforms in handling mulit-user signals when there is imperfect synchronization in time domain. We have provided further discussions and comparisons of CP-OFDM, WOLA-OFDM and BF-OFDM. More precisely, we have considered the coexistence of two users which are asynchronously transmitting in adjacent bands using the same transmit power per subcarrier. We have also provided insights on the impact of several important system parameters, e.g. guard bandwidth and filter design. According the evaluation performed through the developed testbed, we have demonstrated that the discussed filtered (BF-OFDM) and windowed (WOLA-OFDM) waveforms guaranties satisfactory robustness to inter-user interference compared to CP-OFDM. In some specific scenario, the guard band can be considerably reduced achieving a full spectrum utilization.

Based on the experimental testbed results, it is safe to recommend the consideration of BF-OFDM and WOLA-OFDM for the future wireless networks.

REFERENCES

[1] 3rd Generation Partnership Project (3GPP), overall description stage 2, technical specification group access network 38.300, 12 2017, 2.0.0.

[2] Y. Liu, X. Chen, Z. Zhong, B. Ai, D. Miao, Z. Zhao, J. Sun, Y. Teng, and H. Guan. Waveform design for 5g networks: Analysis and comparison. IEEE Access, 5:19282–19292, 2017.

[3] S. Y. Lien, S. L. Shieh, Y. Huang, B. Su, Y. L. Hsu, and H. Y. Wei. 5g new radio: Waveform, frame structure, multiple access, and initial access. IEEE Communications Magazine, 55(6):64–71, 2017.

[4] R. Gerzaguet, S. Bicais, P. Rosson, J. Estavoyer, X. Popon, D. Dassonville, J. B. Dore, B. Miscopein, M. Pezzin, D. Miras, and D. Ktenas. 5g multi-service field trials with bf-ofdm. In 2017 IEEE Globecom Workshops (GC Wkshps), pages 1–5, Dec 2017.

[5] M. Shafi, A. F. Molisch, P. J. Smith, T. Haustein, P. Zhu, P. De Silva, F. Tufvesson, A. Benjebbour, and G. Wunder. 5g: A tutorial overview of standards, trials, challenges, deployment, and practice. IEEE Journal on Selected Areas in Communications, 35(6):1201–1221, June 2017.

[6] 3rd Generation Partnership Project (3GPP), study on new radio (nr) access technology; physical layer aspects, rel. 14, 38.802 v. 14.2.0, 09 2017.

[7] T. Levanen, J. Pirskanen, K. Pajukoski, M. Renfors, and M. Valkama. Transparent tx and rx waveform processing for 5g new radio mobile communications. IEEE Wireless Communications, pages 1–9, 2018.

[8] C. Kim, Y. H. Yun, K. Kim, and J. Y. Seol. Introduction to qam-fbmc: From waveform optimization to system design. IEEE Communications Magazine, 54(11):66–73, November 2016.

[9] C. Zhang and R. C. Qiu. Massive mimo as a big data system: Random matrix models and testbed. IEEE Access, 3:837–851, 2015.

[10] M. Renfors, J. Yli-Kaakinen, T. Levanen, M. Valkama, T. Ihalainen, and J. Vihriala. Efficient fast-convolution implementation of filtered cp-ofdm waveform processing for 5g. In 2015 IEEE Globecom Workshops (GC Wkshps), pages 1–7, Dec 2015.

[11] R1-162199 - Waveform candidates.

[12] H. Cho, Y. Yan, G. K. Chang, and X. Ma. Asynchronous multi-user uplink transmissions for 5g with ufmc waveform. In 2017 IEEE Wireless Communications and Networking Conference (WCNC), pages 1–5, March 2017.

[13] L. Zhang, A. Ijaz, P. Xiao, M. M. Molu, and R. Tafazolli. Filtered ofdm systems, algorithms, and performance analysis for 5g and beyond. IEEE Transactions on Communications, 66(3):1205–1218, March 2018.

[14] R. Zakaria and D. Le Ruyet. Theoretical Analysis of the Power Spectral Density for FFT-FBMC Signals. IEEE Communications Letters, 20(9):1748–1751, Sept 2016.

[15] Robin Gerzaguet, David Demmer, Jean-Baptiste Doré, and Dimitri Kténas. Block-Filtered OFDM: a new promising waveform for multi-service scenarios. In submitted to IEEE ICC 2017 (ICC), Paris, France, May 2017.

[16] Y. Medjahdi, S. Traverso, R. Gerzaguet, H. Shaïek, R. Zayani, D. Demmer, R. Zakaria, J. B. Doré, M. Ben Mabrouk, D. Le Ruyet, Y. Louët, and D. Roviras. On the road to 5g: Comparative study of physical layer in mtc context. IEEE Access, 5:26556–26581, 2017.

[17] S. Dikmese and A. Loulou and S. Srinivasan and M. Renfors. Spectrum sensing and resource allocation models for enhanced OFDM based cognitive radio. In 2014 9th International Conference on Cognitive Radio Oriented Wireless Networks and Communications (CROWNCOM), pages 360–365, June 2014.

[18] S. Dikmese and M. Renfors and I. Guvenc. Flexible filter bank based spectrum sensing and waveform processing for mission critical communications. In MILCOM 2017 - 2017 IEEE Military Communications Conference (MILCOM), pages 174–179, Oct 2017.

[19] J. Yli-Kaakinen, T. Levanen, S. Valkonen, K. Pajukoski, J. Pirskanen, M. Renfors, and M. Valkama. Efficient fast-convolution-based waveform processing for 5g physical layer. IEEE Journal on Selected Areas in Communications, 35(6):1309–1326, June 2017.

[20] P. Guan, D. Wu, T. Tian, J. Zhou, X. Zhang, L. Gu, A. Benjebbour, M. Iwabuchi, and Y. Kishiyama. 5g field trials: Ofdm-based waveforms and mixed numerologies. IEEE Journal on Selected Areas in Communications, 35(6):1234–1243, June 2017.

[21] R. Zayani, H. Shaiek, C. Alexandre, X. Cheng, X. Fu, and D. Roviras. A testbed for experimental performance evaluaion of multicarrier waveforms in presence of rf power amplifier. In 2018 IEEE 15th International

Symposium on Wireless Communication Systems (ISWCS), pages 1–6, August 2018.

[22] X. Lu, L. Ni, S. Jin, C. K. Wen, and W. J. Lu. Sdr implementation of a real-time testbed for future multi-antenna smartphone applications. IEEE Access, 5:19761–19772, 2017.

[23] C. Politis, S. Maleki, J. M. Duncan, J. Krivochiza, S. Chatzinotas, and B. Ottesten. Sdr implementation of a testbed for real-time interference detection with signal cancellation. IEEE Access, 6:20807–20821, 2018.

[24] T. Wattanasuwakull and W. Benjapolakul. Papr reduction for ofdm transmission by using a method of tone reservation and tone injection. In 2005 5th International Conference on Information Communications Signal Processing, pages 273–277, Dec 2005.

[25] V. Cuteanu and A. Isar. Papr reduction of ofdm signals using selective mapping and clipping hybrid scheme. In 2012 Proceedings of the 20th European Signal Processing Conference (EUSIPCO), pages 2551–2555, Aug 2012.

[26] USRP-2942 Specifications, available at: https://www.ni.com/pdf/manuals/374410d.pdf.

[27] Pasternack PE15A4017, available at: https://www.pasternack.com/images/productpdf/pe15a4017.pdf.

[28] N. C. Beaulieu and P. Tan. On the effects of receiver windowing on ofdm performance in the presence of carrier frequency offset. IEEE Transactions on Wireless Communications, 6(1):202–209, Jan 2007.

[29] I. Gaspar, M. Matthé, N. Michailow, L. Leonel Mendes, D. Zhang, and G. Fettweis. Frequency-shift offset-qam for gfdm. IEEE Communications Letters, 19(8):1454–1457, Aug 2015.

[30] David Demmer, Robin Gerzaguet, Jean-Baptiste Doré, Didier Le Ruyet, and Dimitri Kténas. Block-Filtered OFDM: an exhaustive waveform to overcome the stakes of future wireless technologies. In submitted to IEEE ICC (ICC), Paris, France, May 2017.

[31] M. Bellanger. New applications of digital signal processing in communications. IEEE ASSP Magazine, 3(3):6–11, Jul 1986.

[32] D. Demmer, R. Gerzaguet, J. B. Doré, D. Le Ruyet, and D. Kténas. Block-filtered ofdm: A novel waveform for future wireless technologies. In 2017 IEEE International Conference on Communications (ICC), pages 1–6, May 2017.

[33] D. Demmer, R. Gerzaguet, J. B. Doré, D. Le Ruyet, and D. Kténas. Filter design for 5g bf-ofdm waveform. In 2017 European Conference on Networks and Communications (EuCNC), pages 1–5, June 2017.

[34] Seung Hee Han and Jae Hong Lee. An overview of peak-to-average power ratio reduction techniques for multicarrier transmission. IEEE Wireless Communications, 12(2):56–65, April 2005.

[35] S. S. K. C. Bulusu, M. Crussière, J. F. Hélard, R. Mounzer, Y. Nasser, O. Rousset, and A. Untersee. Quasi-optimal tone reservation papr reduction algorithm for next generation broadcasting systems: A performance/complexity/latency tradeoff with testbed implementation. IEEE Transactions on Broadcasting, pages 1–7, 2018.

[36] R. W. Bauml, R. F. H. Fischer, and J. B. Huber. Reducing the peak-to-average power ratio of multicarrier modulation by selected mapping. Electronics Letters, 32(22):2056–2057, Oct 1996.

[37] Hanen Bouhadda, Hmaied Shaiek, Daniel Roviras, Rafik Zayani, Yahia Medjahdi, and Ridha Bouallegue. Theoretical analysis of ber performance of nonlinearly amplified fbmc/oqam and ofdm signals. EURASIP Journal on Advances in Signal Processing, 2014(1):60, 2014.

[38] Jian Li and Jacek Ilow. Adaptive volterra predistorters for compensation of non-linear effects with memory in ofdm transmitters. In Communication Networks and Services Research Conference, 2006. CNSR 2006. Proceedings of the 4th Annual, pages 4–pp. IEEE, 2006.

[39] Anding Zhu and Thomas J Brazil. An adaptive volterra predistorter for the linearization of rf high power amplifiers. In Microwave Symposium Digest, 2002 IEEE MTT-S International, volume 1, pages 461–464. IEEE, 2002.

[40] Tong Wang and Jacek Ilow. Compensation of nonlinear distortions with memory effects in ofdm transmitters. In Global Telecommunications Conference, 2004. GLOBECOM'04. IEEE, volume 4, pages 2398–2403. IEEE, 2004.

[41] Lei Ding, Raviv Raich, and G Tong Zhou. A hammerstein predistortion linearization design based on the indirect learning architecture. In Acoustics, Speech, and Signal Processing (ICASSP), 2002 IEEE International Conference on, volume 3, pages III–2689. IEEE, 2002.

[42] Muhammad A Nizamuddin, Philip J Balister, William H Tranter, and Jeffrey H Reed. Nonlinear tapped delay line digital predistorter for power amplifiers with memory. In Wireless Communications and Networking, 2003. WCNC 2003. 2003 IEEE, volume 1, pages 607–611. IEEE, 2003.

[43] Terry Hoh, Ge Jian-hua, Geng Shu-jian, and Wang Gang. A nonlinearity predistortion technique for hpa with memory effects in ofdm systems. Nonlinear Analysis: Real World Applications, 8(1):249–256, 2007.

[44] P Jardin and G Baudoin. Filter look up table method for power amplifiers linearization. IEEE transaction on Vehicular technology, 56(3):1076–1087, 2007.

[45] Rafik Zayani, Ridha Bouallegue, and Daniel Roviras. Adaptive predistortions based on neural networks associated with levenberg-marquardt algorithm for satellite down links. EURASIP J. Wirel. Commun. Netw., 2008:2:1–2:15, January 2008.

[46] R. Zayani, Y. Medjahdi, H. Bouhadda, H. Shaiek, D. Roviras, and R. Bouallegue. Adaptive predistortion techniques for non-linearly amplified fbmc-oqam signals. In 2014 IEEE 79th Vehicular Technology Conference (VTC Spring), pages 1–5, May 2014.

[47] P. N. Landin and D. Rönnow. Rf pa modeling considering odd-even and odd order polynomials. In 2015 IEEE Symposium on Communications and Vehicular Technology in the Benelux (SCVT), pages 1–6, Nov 2015.

[48] D. Zhou and V. E. DeBrunner. Novel adaptive nonlinear predistorters based on the direct learning algorithm. IEEE Transactions on Signal Processing, 55(1):120–133, Jan 2007.

[49] Lei Ding, G. T. Zhou, D. R. Morgan, Zhengxiang Ma, J. S. Kenney, Jaehyeong Kim, and C. R. Giardina. A robust digital baseband predistorter constructed using memory polynomials. IEEE Transactions on Communications, 52(1):159–165, Jan 2004.

RAFIK ZAYANI (M'09) received the Engineer, M.Sc. and Ph.D. degrees from the ÃL'cole Nationale dâĂŹIngÃl'nieurs de Tunis (ENIT) in 2003, 2004, and 2009, respectively. He was with the Laboratory of Communications Systems (SysâĂŹCom), ENIT, from 2003 to 2005. Since 2005, he has been with the InnovâĂŹCOM laboratory, SupâĂŹCom School, Tunisia. From 2004 to 2009, he was with the Department of Telecommunication and Networking, Institut SupÃl'rieur dâĂŹInformatique (ISI), Tunis, as a contractual Assistant Professor. Since 2009, he has been an Associate Professor (tenure position) with the ISI, Tunisia. Since 2010, he has been an Associate Researcher with the CEDRIC Laboratory, Conservatoire National des Arts et MÃl'tiers, France. He is an Established Researcher with long experience in multicarrier communications, energy efficiency enhancement by: transmitter linearization techniques (baseband DPD) and PAPR reduction; high power amplifier characterization; neural network; identification modeling and equalization; and MIMO technologies. He was involved in enhanced multicarrier waveforms, such as FBMC-OQAM, UFMC, GFDM, BF-OFDM, and WOLA-OFDM. He has contributed in several European (EMPHATIC) and French (WONG5) projects that aim at designing flexible air-interfaces for future wireless communications (5G and Beyond). He has recently been awarded a H2020 MSCA IF grant for his ADMA5 project proposal.

This article has been accepted for publication in a future issue of this journal, but has not been fully edited. Content may change prior to final publication. Citation information: DOI 10.1109/ACCESS.2018.2879375, IEEE Access

HMAIED SHAIEK received the Engineer degree from the National Engineering School of Tunis in 2002, and the masterâĂŹs degree from the UniversitÃl' de Bretagne Occidentale in 2003, and the Ph.D. degree from the Lab-STICC CNRS Team, Telecom Bretagne, in 2007. He was with Canon Inc., until 2009. He left the industry to integrate with the ÃL'cole Nationale dâĂŹIngÃl'nieurs de Brest as a Lecturer, from 2009 to 2010. In 2011, he joined the CNAM, as an Associate Professor in electronics and signal processing. He has authored or co-authored three patents, six journal papers, and over 25 conference papers. His research activities focus on performances analysis of multicarrier modulations with nonlinear power amplifiers, PAPR reduction, and power amplifier linearization. He contributed to the FP7 EMPHATIC European project and is involved in two national projects, such as Accent5 and Wong5, funded by the French National Research Agency. He has co-supervised three Ph.D. students and four master students.

XINYING CHENG received her B.Sc. degree in Measuring Control Technology Instruments from Southeast University, Nanjing, China in 2017. She is now a master student in Telecommunication and Network at Conservatoire National des Arts et MÃl'tiers (CNAM), France. She is now working in CEDRIC Laboratory, CNAM, France. Her research interests are in physical layer design, including waveform, MIMO, etc. for the next generation of communication.

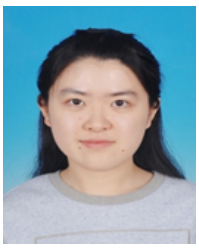

XIAOTIAN FU received engineering degree from Southeast University, Nanjing, in 2017. She is a Master 2 student and doing internship of at CEDRIC Laboratory, Conservatoire National des Arts et MÃl'tiers (CNAM), France. Her research interest lies in wireless communication waveforms for 5G networks.

CHRISTOPHE ALEXANDRE was born in France on December 22, 1963. He received the Engineering degree, Master degree and Ph.D. degree in electronics from the Conservatoire National des Arts et MÃl'tiers (CNAM) of Paris, France, in 1992, 1992 and 1995, respectively. He is Associate Professor since 1996 in the electrical engineering Department and CEDRIC Laboratory, CNAM. His research interests include digital design with FPGA, embedded electronics, ADC/DAC and radio receivers.

DANIEL ROVIRAS was born in 1958. He received the Engineer degree from SUPELEC, Paris, France, in 1981, and the Ph.D. degree from the National Polytechnic Institute of Toulouse, Toulouse, France, in 1989. He spent in the industry as a Research Engineer for seven years. He joined the Electronics Laboratory, ÃL'cole Nationale SupÃl'rieure dâĂŹÃL'lectrotechnique, dâĂŹÃL'lectronique, dâĂŹInformatique, et des TÃl'lÃl'communications (ENSEEIHT). In 1992, he joined the Engineering School, ENSEEIHT, as an Assistant Professor, where he has been a Full Professor since 1999. Since 2008, he has been a Professor with the Conservatoire National des Arts et MÃl'tiers (CNAM), Paris, France, where his teaching activities are related to radiocommunication systems. He is currently a member of the CEDRIC Laboratory, CNAM. His research activity was first centered around transmission systems based on infrared links. Since 1992, his topics have widened to more general communication systems, such as mobile and satellite communications systems, equalization, and predistortion of nonlinear amplifiers, and multicarrier systems.